Available online at www.sciencedirect.com
SCIENCE DIRECT®
Polymer 44 (2003) 6973–6988
polymer
www.elsevier.com/locate/polymer

Structural changes in isothermal crystallization process of polyoxymethylene investigated by time-resolved FTIR, SAXS and WAXS measurements

Hisakatsu Hama, Kohji Tashiro*

Department of Macromolecular Science, Graduate School of Science, Osaka University, Toyonaka, Osaka 560-0043, Japan

Received 8 May 2003; received in revised form 9 July 2003; accepted 5 August 2003

Abstract

Structural evolution in the isothermal crystallization process of polyoxymethylene from the molten state has been investigated by carrying out the time-resolved measurements of infrared spectra and synchrotron small angle X-ray scattering (SAXS) and wide angle X-ray scattering. In case of isothermal crystallization at 130 °C, for example, the infrared bands intrinsic of folded chain crystal (FCC) morphology appeared at first, and then the bands of extended chain crystal (ECC) morphology were detected with time delay of ca. 150 s. In the SAXS experiment at 130 °C, the lamellar stacking structure of the long period of ca. 15 nm was observed at first, which changed rapidly to ca. 12 nm in a short time. The SAXS peak with the long period of ca. 6 nm started to appear with a time delay of ca. 150 s after the initial lamellae appeared and coexisted with the initially-observed 12 nm peak. Judging from the timing to detect these characteristic infrared and SAXS signals, a good correspondence was found to exist between the stacked lamellar structure of 12 nm long period and FCC morphology and between the structure of 6 nm long period and ECC morphology. The quantitative analysis was made for the SAXS data on the basis of the lamellar insertion model combined with the paracrystalline theory of the second-kind of disorder. The following structural evolution was deduced from all these results. Immediately after the temperature jump from the melt to 130 °C, the stacked lamellar structure of FCC morphology was generated at first. New lamellae were formed from the amorphous region in between the originally-existing lamellae about 150 s later, where the random chain segments bridging the adjacent lamellae were extended to form the taut tie chains, giving infrared bands of ECC morphology. This inserted lamellar structure of 6 nm long period coexisted at a population of ca. 6% with the initially-formed lamellar stacking structure of 12 nm long period. When the experiment was made at 150 °C, only the formation of stacked lamellar structure of FCC morphology was observed and the insertion of new lamella did not occur.

Keywords: Polyoxymethylene; Isothermal crystallization; Folded chain crystal

1. Introduction

Polyoxymethylene (POM) is one of the most important engineering plastics which have been used in various fields. In order to understand the relationship between structure and physical properties of POM from the microscopic point of view, we need to clarify not only the static aggregation structure of molecular chains but also the evolution process of such a structure. Although many papers have been reported so far about the static structure of POM from the molecular level to the higher-order structure level [1–26], the details of the structural evolution process have not yet been enough well clarified [12–26]. This situation may come from various problems encountered in performing the experiment actually. For example, POM is easy to thermally decompose at high temperature above the melting point. In order to avoid this problem, a utilization of a copolymer with small amount of other kind of comonomer may be useful as long as the crystallization behavior is not affected seriously. Another example is seen in the purity of POM sample. Of course, POM has molecular weight distribution. In addition, the POM produced by a cationic polymerization of trioxane is said to contain some amount of macrocyclic compounds [27,28]. Such macrocyclic compounds might play a role in the crystallization process from the molten state.

In the previous papers [29,30] we carried out the measurements of infrared spectra and wide- and small-angle

* Corresponding author.

0032-3861/$ - see front matter © 2003 Elsevier Ltd. All rights reserved.
doi:10.1016/j.polymer.2003.08.019

X-ray scatterings (WAXS and SAXS, respectively) in the slow cooling process from the melt to room temperature. The infrared spectra of POM are known to be highly sensitive to the morphology of the crystallites [31,32]. In the cooling process from the melt we found that the infrared bands characteristic of folded chain crystal (FCC) morphology appeared around 156 °C, followed by a gradual increase of infrared bands of extended chain crystal (ECC) around 140 °C [29]. The quantitative analysis of SAXS data clarified the formation of stacked lamellar structure with long period of ca. 14 nm around 155 °C and the insertion of new lamellae in between the originally existing lamellae at the secondary crystallization stage below 140 °C [30]. As a result, the long period changed to a half, from 14 to 7 nm, in some parts of stacked lamellar structure. An ideal model of this inserted lamellar structure is illustrated in Fig. 1(c). In the actual sample these two types of lamellar stacking structure coexist together at a certain probability [30].

Another problem to be solved is the formation process of lamellar stacking structure of POM in the isothermal crystallization from the melt. Since the main SAXS peak characteristic of the FCC morphology is generated around 155 °C and the secondary lamellae inserted to the original lamellar structure are formed around 140 °C, it is expected that we may be able to observe the different crystallization behavior in the isothermal crystallization process at different temperature when we carry out the time-resolved infrared and SAXS measurements, as will be described in the present paper. The combination of SAXS, WAXS and infrared spectral data allows us to obtain the concrete structural change in isothermal crystallization process viewed from molecular level as well as higher order structure level. This type of study was reported for the isothermal crystallization phenomenon of polyethylene [33–35], but has never been made for POM.

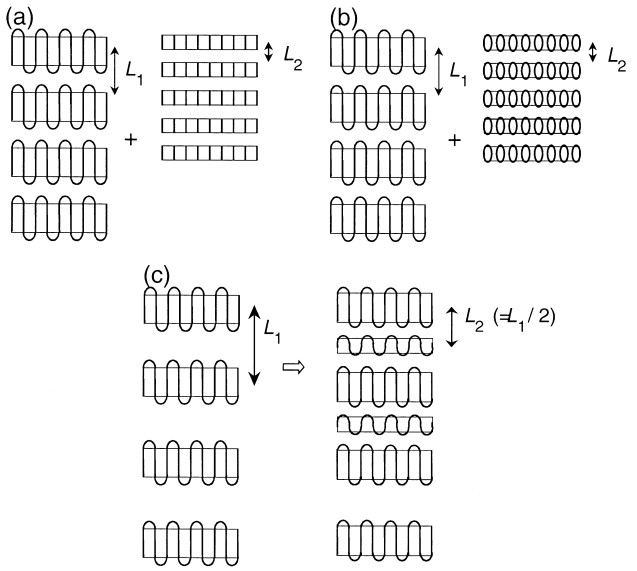

Fig. 1. Illustrated models of stacked lamellar structures. (a) Coexistence of the main lamellar stacking structure (L_1) and the stacked lamellae of linear low-molecular-weight compounds (L_2), (b) coexistence of the main lamellar stacking structure (L_1) and the stacked lamellae of macrocyclic compounds (L_2), and (c) an insertion model of new lamellae in between the already-existing lamellar stacking structure.

2. Experimental

2.1. Material

POM samples employed here were the same with those reported in the previous papers: the copolymer of trioxane with small content of ethylene oxide (ca. 2.2 wt%, Duracon M90, Polyplastics Co. Ltd, Japan) [29,30]. This sample was used in order to avoid the thermal decomposition as much as possible without any loss of characteristic crystallization behavior of POM homopolymer itself, although the melting and crystallization temperatures were about 5 °C lower than those of the homopolymer. The M_w was ca. 69,300 g/mol and M_w/M_n ca. 2.3.

2.2. Measurements

2.2.1. Thermal analysis

DSC thermograms were measured by a Perkin–Elmer Pyris 1 to estimate the thermal behavior in the isothermal crystallization process. The sample packed into an aluminum pan was cooled rapidly at a rate of ca. 500 °C/min from 205 to 130 or 150 °C, and the time dependence of thermal energy was measured. The thus-obtained thermogram was analyzed to evaluate the evolution of crystallinity as a function of time.

2.2.2. FTIR measurement

Infrared spectra were measured by using a Bio Rad FTS-60A/896 Fourier-transform infrared spectrometer at a resolution power 2 cm^{-1}. The sample was sandwiched between a pair of thin KBr plates and set into an optical cell designed for an isothermal crystallization experiment. The details of this cell were already reported in Ref. [36]. The sample was heated to 205 °C and then jumped to the hot plate kept at 130 or 150 °C (T_c). The rate of temperature jump was about 1000 °C/min. The temperature fluctuation at T_c was about ±0.1 °C. The infrared spectra were measured at every ca. 4 s in a rapid scanning mode.

2.2.3. SAXS and WAXS measurements

Time dependences of SAXS and WAXS were measured by using a synchrotron radiation as an X-ray source at the beam lines BL10C and BL15A, respectively, of the Photon Factory at the KEK (High-Energy Accelerator Research Organization) in Tsukuba, Japan. The wavelength of incident X-ray beam was 0.149 nm in both of BL10C and BL15A. The sample was packed to a small metal holder and set in a temperature jump apparatus, the details of which were described in Refs. [34,37]. The X-ray scattering data

were collected at every 3 s in both the SAXS and WAXS measurements. The detector was a one-dimensional Position Sensitive Proportional Counter (PSPC) for both the measurements. In the analysis of SAXS and WAXS data, correction of background and fluctuation of beam intensity were made. The X-ray beam was almost round at the sample position and therefore no correction was made for an effect of beam shape. The scattering intensity $I(q)$ was transformed to $I(q)q^2$ for the correction of Lorentz factor, where q was a scattering vector defined as $q = 4\pi \sin\theta/\lambda$ (λ wavelength of incident X-ray beam and 2θ: scattering angle).

3. Results and discussion

3.1. Brief review on slow cooling process

Before the experimental results are reported here on the time-resolved measurements in the isothermal crystallization process, it may be useful to review the experimental data collected in the non-isothermal crystallization or slow cooling process from the melt [29,30] although the result was already mentioned briefly in Section 1.

In that experiment the infrared spectra and SAXS/WAXS data were measured stepwise in the slow cooling process from the melt. Around 155 °C the infrared bands characteristic of FCC morphology were detected. In the SAXS experiment, the peak of long period of 17 nm and lamellar thickness of 4.2 nm were observed. With decreasing temperature, the long period changed to 14 nm. Below 140 °C a new SAXS peak was observed at a position of long period of ca. 7 nm and coexisted with the initially-observed SAXS peak, the intensity of which became weaker in parallel. In almost the same temperature region, the infrared bands of ECC were found to appear. Since the ECC bands were detected in the same temperature region as the observation of the SAXS peak with the 7 nm long period, the ECC may have some structure relation with the change of the lamellar stacking structure. As a possibility, the structural change shown in Fig. 1(c) was proposed. In the cooling process from the melt, the stacked lamellar structure with long period 14 nm was created at first. When the sample was cooled down to ca. 140 °C, the amorphous region in the stacked lamellae was crystallized to form new lamellae. As a result the long period changed to 7 nm. At non-zero probability some of the chains might pass through the neighboring lamellae and they might be included into a newly created lamella, resulting in the formation of fully-extended chain segments passing through the several numbers of stacked lamellae. These straight parts might be assumed as taut tie chains and give the 'ECC-like' morphology. It should be noted here the model shown in Fig. 1(c) is too ideal to reflect the actual structure of the system. The stacked lamellar structure of 7 nm long period is existent at a population of ca. 30% at most and the remaining part consists of the originally-created lamellar structure with 14 nm long period.

Some opinions might be there about the assignment of the second peak of SAXS with the long period 7 nm. For example, this peak should be the second-order peak of the first peak. This possibility was erased because the temperature dependence of the first and second peaks was different from each other as mentioned above. More detailed discussion will be made about this point in a later section. As the next opinion, the second peak might be assigned to the layer stacking structure of low-molecular-weight components of POM [23]. Since the infrared bands of ECC morphology were found to correspond to this second SAXS peak [30], it might be possible to say that the low-molecular-weight components are stacked with an averaged long period of ca. 7 nm to form an ECC structure (Fig. 1(a)). But the comparable intensities of the first and second SAXS peaks, as observed at room temperature, suggest the coexistence of both the FCC lamellar structure and ECC structure in comparable amounts. This means that the molecular weight distribution of the used POM sample ($M_w = 69,300$ g/mol, $M_w/M_n = 2.3$) is bimodal between the high-molecular-weight component of 137,500 g/mol and the low-molecular-weight component of 1100 g/mol with an almost equal population. This is curious from the GPC result [27]: the low-molecular-weight linear component is negligible. It is also inconsistent with the fact that all the samples with different M_w and M_w/M_n show the similar SAXS patterns [30]. Another possibility is an existence of macrocyclic compounds in the POM sample (Fig. 1(b)). Because of the backbiting reactions occurring at a certain probability in the cationic polymerization system of trioxane [27,28], some amounts of macrocyclic compounds are said to be produced in addition to the long linear POM chains. But, the study of infrared spectra revealed that the macrocyclic compounds give the infrared bands of FCC morphology [38], inconsistent with the correspondency between the SAXS second peak and infrared ECC bands. Besides, the possibility of macrocyclic compounds to contribute to the SAXS second peak can be denied because of the similar reasons mentioned above for the linear low-molecular-weight compounds. In this way, we do not have any positive experimental data to assign the SAXS second peak to the low-molecular-weight compounds and/or macrocyclic compounds. More detailed discussion about the quantitative interpretation of SAXS data will be made in a later section.

3.2. Time dependence of DSC thermogram

Time dependences of DSC thermograms were measured in the isothermal crystallization at 130 and 150 °C, from which the fraction of enthalpy change $\Delta H(t)/\Delta H_{total}$, where $\Delta H(t)$ was an enthalpy change from the start to time t and ΔH_{total} was the total enthalpy change, or the evolution of relative crystallinity was estimated (refer to Figs. 5 and 6).

As the time passed, the relative crystallinity increased steeply after some induction period (4 s at 130 °C and 24 s at 150 °C). The increasing rate was higher at 130 than 150 °C.

3.3. Time dependence of IR spectra

The time dependence of infrared spectra was measured in the isothermal crystallization process at 130 and 150 °C from the melt as shown in Figs. 2 and 3, respectively. In Fig. 2, the spectrum measured at 0 s corresponds to that of the molten state, where 0 s was defined as a time when the temperature reached the predetermined value after jump. As the time passed, the bands characteristic of FCC were detected at first around 4 s and steeply increased in intensity. The band at 902 cm^{-1} is due to the ECC morphology, which began to appear around 150 s and increased in intensity gradually. When the sample was cooled to 150 °C from the melt, the FCC bands were detected at 24 s from the temperature jump and increased in intensity gradually as seen in Fig. 3. In this case no ECC band was observed at any time.

These spectral data were analyzed quantitatively to estimate the time dependence of the ECC and FCC band intensity. Since many bands were overlapped together, the evaluation of intensity change was difficult. As discussed in detail in the previous paper [29], the observed spectra were differentiated twice with respect to wavenumber in order to get the second derivatives of the spectral profiles. The peak corresponding to the infrared band of the molten state was observed at ca. 907, 1110 and 1218 cm^{-1} in the second derivatives curves at both of the temperatures 130 and 150 °C. In the analysis of second derivatives curves at

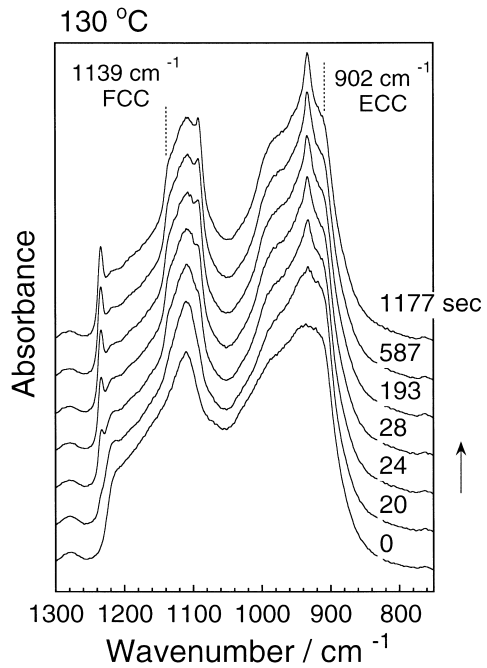

Fig. 2. Time dependence of infrared spectra of POM taken in the isothermal crystallization process at 130 °C.

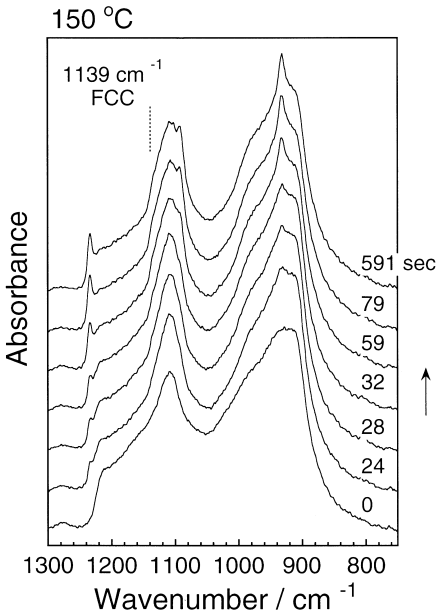

Fig. 3. Time dependence of infrared spectra of POM taken in the isothermal crystallization process at 150 °C.

130 °C, the peak corresponding to the 902 cm^{-1} ECC band was found to increase in height with a passage of time as shown in Fig. 4(a), where the ECC peak should be distinguished from the peak due to the melt (a comparison of the peak profile change between 130 and 150 °C helps us to make the difference clearer). But, in the case of crystallization at 150 °C, only the peak corresponding to the melt was observed with a slight decrease in height along with the evolution of FCC bands. In Figs. 5 and 6 is plotted the thus evaluated second derivative intensity against time for both the bands of ECC at 902 cm^{-1} and FCC at 1139 cm^{-1} in comparison with the DSC data. In the isothermal crystallization process at 130 °C, the FCC band at 1139 cm^{-1} started to appear at ca. 4 s and increased in intensity quite steeply. The ECC band at 902 cm^{-1} appeared at a later time than the FCC band, around 150 s, and grew up slowly with a passage of time. At 150 °C, the FCC band intensity increased gradually but no ECC band appeared. Sharp increase in crystallinity estimated from the DSC data was found to correspond well to the appearance of the FCC band. The gradual change in ECC band intensity may correspond to the broad background of the DSC thermogram, but the details are not clear [29].

The different behavior of FCC and ECC morphologies in the isothermal crystallization will be interpreted in a later section by combining the infrared data with the time-resolved SAXS/WAXS experimental data.

3.4. Time dependence of SAXS profiles

The SAXS profiles collected in the isothermal crystallization process at 130 °C are reproduced in Fig. 7. Around 11 s after jump, a peak L_1 started to appear and increased in

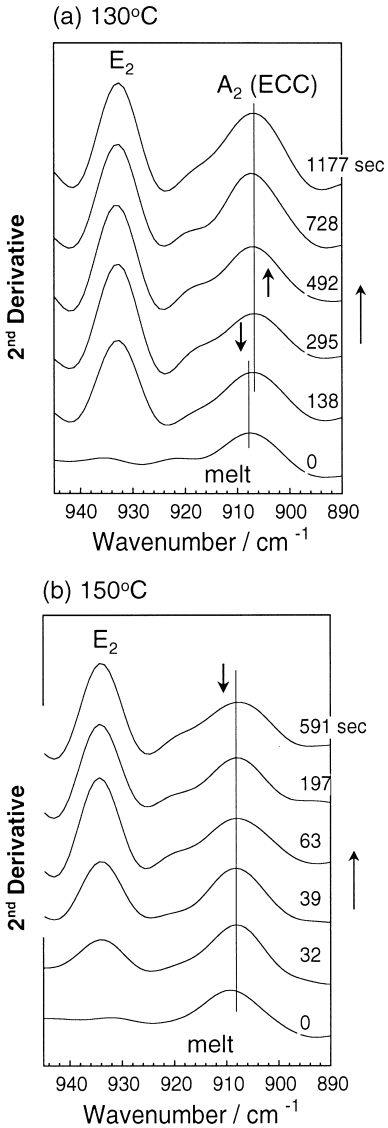

Fig. 4. Time dependence of the second derivatives profile of infrared spectra. (a) 130 °C and (b) 150 °C.

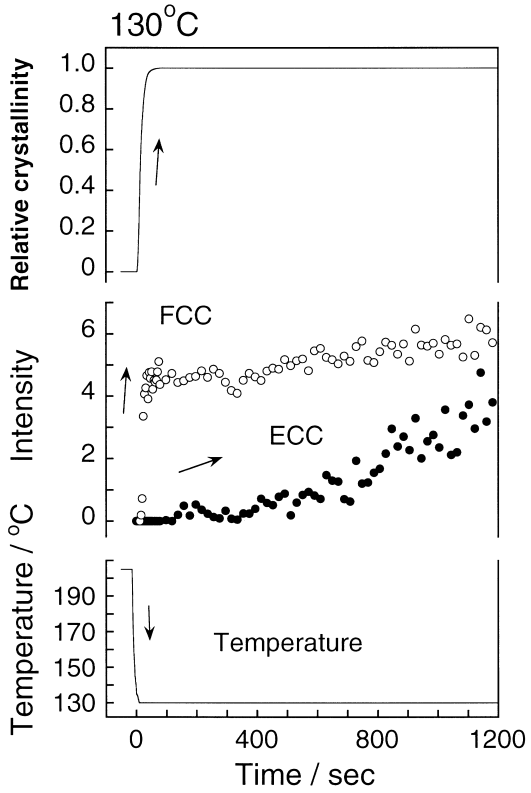

Fig. 5. Time dependence of the infrared band intensity estimated from the second derivatives curves in comparison with the ratio $\Delta H(t)/\Delta H_{\text{total}}$ or the degree of relative crystallinity derived from the DSC thermogram in the isothermal crystallization process at 130 °C.

intensity with slight shift of the peak position toward higher q side. The peak had a shoulder at higher q side and this shoulder becomes weaker with the passage of time. At the same time a broad peak was also observed around $q = 1.1\ \text{nm}^{-1}$, although it is too low in height and noisy. In the time region of 150 s another peak L_2 started to appear around $q = 0.9\ \text{nm}^{-1}$ and increased in intensity gradually. In parallel the intensity of the L_1 peak decreased and became more comparable to that of the L_2 peak at 1200 s (this tendency was more remarkable when the sample was cooled down to room temperature [30]). The long periods estimated for the L_1 and L_2 peaks at the terminal point of the experiment (1438 s) are 12.1 and 6.5 nm, respectively; the L_1 being almost twice the L_2. This type of SAXS profile change was not detected when the isothermal crystallization was performed at 150 °C. The time dependence of SAXS profile measured at 150 °C is shown in Fig. 8. Around 35 s after jump, a peak L_1 started to appear and increased in intensity with slight shift of the peak position toward higher q side. The L_2 peak could not be observed here. A broad and weak peak was detected around $q = 0.8–1.3\ \text{nm}^{-1}$ in a later stage of crystallization.

3.4.1. Choice of reasonable lamellar stacking model

As discussed in the previous paper [30], we may have various kinds of structural model to interpret the observed SAXS profiles reasonably. In the present paper we check this problem again from a little different point of view.

When the SAXS data collected at 130 °C are viewed, it might be assumed that the L_2 is the second-order peak of the L_1 judging from the relation of long periods L_1 and L_2 ($L_1/L_2 \sim 2$). If it is so, then how can we interpret the change of relative intensity between the L_1 and L_2 peaks in the crystallization process? Schultz et al. [39] calculated the SAXS intensities of the first and second-order peaks for the one-dimensional lamellar stacking structure and showed that the relative intensity of these two peaks can be changed by changing the lamellar thickness or, more strictly speaking, by changing the ratio of the thickness to the long period (the detail of this change is shown in Appendix A in the present paper). But, the L_2 peak height cannot exceed the L_1 peak height even when the lamellar thickness is increased to the value closer to the long period. In the

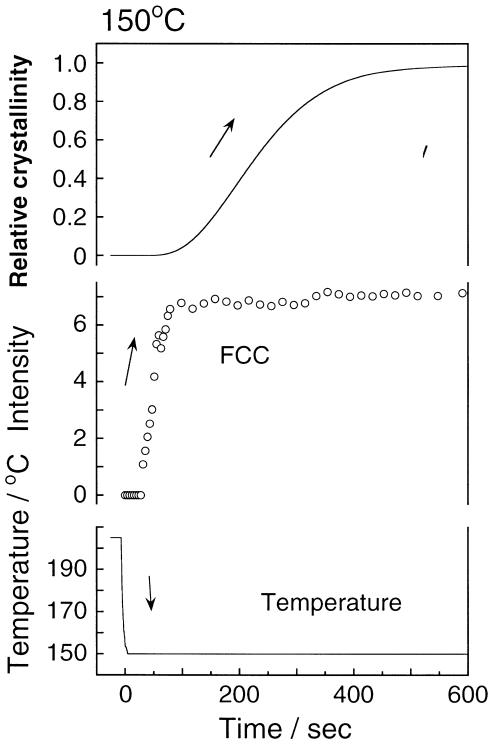

Fig. 6. Time dependence of the infrared band intensity estimated from the second derivatives curves in comparison with the ratio $\Delta H(t)/\Delta H_{\text{total}}$ or the degree of relative crystallinity derived from the DSC thermogram in the isothermal crystallization process at 150 °C.

SAXS experiment made for polyethylene in the isothermal crystallization we observed that the L_2 peak height exceeded the L_1 peak height when the highly-crystalline sample was used [34]. This observation cannot be interpreted simply in

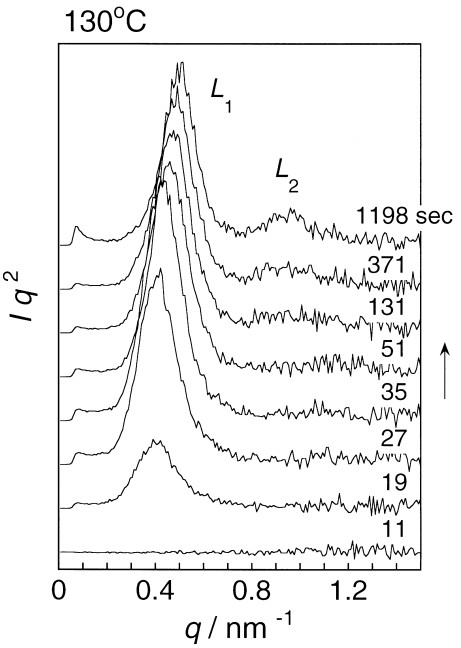

Fig. 7. Time dependence of SAXS profile of POM sample measured in the isothermal crystallization process at 130 °C.

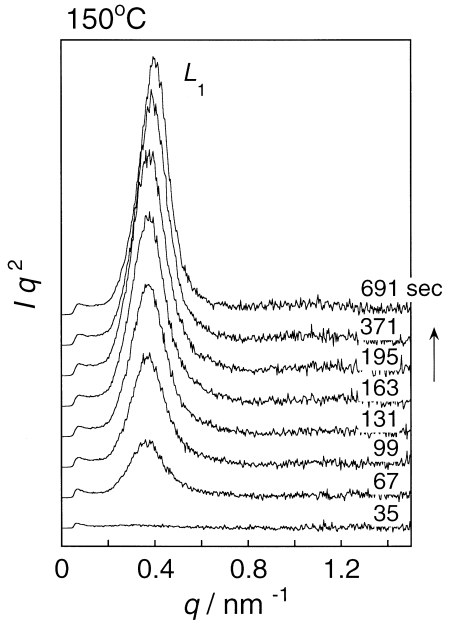

Fig. 8. Time dependence of SAXS profile of POM sample measured in the isothermal crystallization process at 150 °C.

terms of the growth of lamellar thickness. Of course the case of POM might not be the same as polyethylene. But, judging from the similar behavior of SAXS profile and many other experimental data concerning the crystallization phenomenon, it may be more reasonable to assume that these polymers (and other polymers [40–49]) exhibit the essentially same mechanism as for the formation of stacked lamellar structure. That is to say, the concept of increasing lamellar thickness is necessary for the analysis of the SAXS profile change, but it has a limit to apply to the observed relative intensity change between the L_1 and L_2 SAXS peaks. As a trial we fitted the SAXS profile observed at room temperature (in the experiment of slow cooling from the melt [30]) by using a scattering equation derived for the one-dimensionally stacked lamellar structure with the variable lamellar thickness, but the thus-obtained total number of repeating lamellae was 2, quite unrealistic lamellar stacking structure (Appendix A)! We applied also the scattering equation derived for the stacked lamellar structure with the second-kind of paracrystalline disorder [50], where the total number of lamellae was infinite but the stacking regularity was statistically disordered and the correlation between the neighboring lamellae disappeared actually beyond some distance. We could not have any good result as long as we adhered to the model of only one type of lamellar stacking structure. Rather the SAXS profile change observed at 130 °C (Fig. 7) can be reproduced reasonably on the basis of lamellar insertion model as already described in the previous papers [30,34], where the adjustable parameters used are long period, thickness of the two kinds of lamella and the corresponding electron densities. Of course, the SAXS profiles without additional L_2 peak, that is, the SAXS data obtained in the earliest stage of crystallization at

130 °C and those at 150 °C can be analyzed on the basis of a stacked lamellar structure model without any lamellar insertion, but they can be covered by the insertion model with null contribution of the L_2 structure. The details of the discussion made in this paragraph are described more concretely in Appendix A.

3.4.2. SAXS data analysis

As mentioned above, we assume here a model of the two-stage crystallization of stacked lamellar structure in order to make a reasonable interpretation of the observed L_1 and L_2 peaks. The first stage is an appearance of lamellar stacking structure with the long period L_1 and the second stage is an insertion of a new lamella into the already-existing lamellae of L_1 (Fig. 1(c)). As for the insertion of lamellae, there might be several ways to satisfy such a model as shown in Fig. 9(a) [30]. Model I is a regular insertion of new lamellae. The relative height indicates the probability of existence of these lamellae. Model II is similar to model I but the growing timing of lamella is different depending on the position. In model III the new lamella starts to appear from one end and evolves into the direction of the other end. Model IV shows the random insertion of new lamellae. Theoretical calculation revealed that all of these models give essentially the same SAXS patterns (Fig. 9(b)). For the data analysis, we choose the model I in Fig. 9(a) because the structure is periodic and is convenient for the derivation of concrete equation as well as for the determination of structural parameters. In the actual system, the lamellar stacking structure may be more or less disordered [50–59] and the perfectly-filled lamellar parts and the not-yet-filled parts are considered to coexist together (model IV).

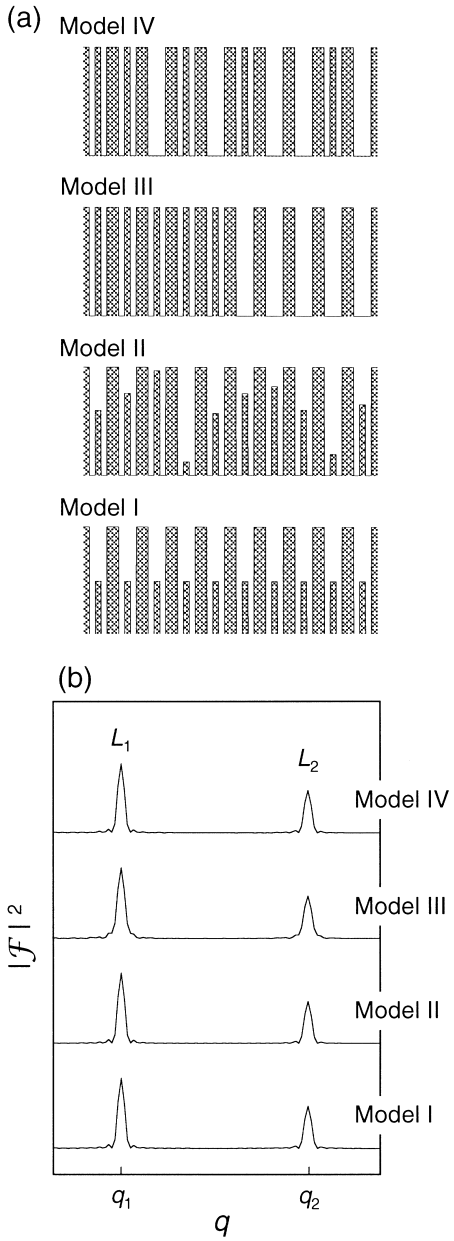

Fig. 9. (a) Various types of lamellar insertion model. Model I: inserted lamellae grow simultaneously at all the positions, Model II: growing timing of inserted lamellae is random, Model III: inserted lamella starts to appear from one end and evolves in the direction of other end, and Model IV: inserted lamellae exist in random fashion. (b) The SAXS profiles calculated for these models. It should be noticed that all the models in (a) give essentially the same pattern with each other.

Model I in Fig. 9(a) is redrawn in Fig. 10 to define the structural parameters clearly. Sometimes the gradually decreasing electron density distribution is introduced in a boundary between lamella and amorphous region [50–59], but the essential result is not changed even when the perfectly rectangular shape is assumed of the electron density distribution of a lamella. The scattering intensity $I(q)$ for this model is given as

$$I(q) = P(q)L(q) \tag{1}$$

where $P(q)$ is a particle factor and $L(q)$ is a lattice factor [51]. $P(q)$ is a square of Fourier-transformation of the basic structure unit of a lamella. $L(q)$ is a square of Fourier-transformation of one-dimensional periodicity with second-kind of paracrystalline disorder [50]. The $P(q)$ and $L(q)$

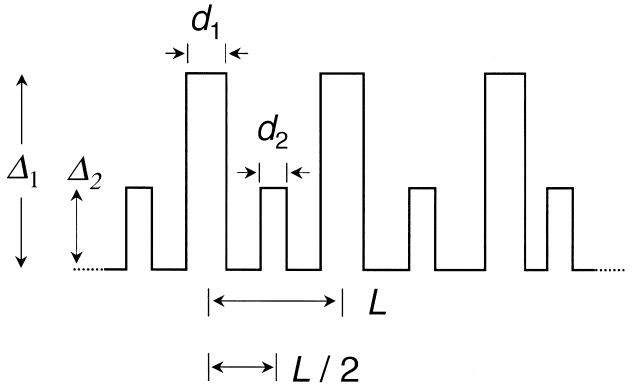

Fig. 10. Lamellar insertion model used for calculation of scattering intensity. Δ_1 is the difference of electron density between the main crystallite and the amorphous phase, Δ_2 is the electron density difference between the inserted lamella and the amorphous phase. d_1 is the thickness of main lamella and d_2 is the thickness of inserted lamella. L is the periodicity between main lamellae.

were derived concretely as shown below

$$P(q) = \left|\int_{-\infty}^{\infty} \rho(x)\mathrm{e}^{-iqx}\mathrm{d}x\right|^2$$
$$= 4[\Delta_1^2 \sin^2(d_1q/2) + 2\Delta_1\Delta_2 \cos(Lq/2)\sin(d_1q/2)$$
$$\sin(d_2q/2) + \Delta_2^2 \sin^2(d_2q/2)]/q^2 \quad (2)$$

where $\rho(x)$ is an electron density function. Δ_1 is the difference of electron density between the main crystalline phase and amorphous phase, Δ_2 is the electron density difference between the inserted lamella, which is sandwiched between main lamellae, and the amorphous phase. d_1 is the thickness of main lamella, d_2 is the thickness of inserted lamella and L is the lamellar periodicity or long period. It was assumed that an inserted lamella exists at the half position of the two neighboring original lamellae.

$$L(q) = \frac{1 - \exp(-4\pi^2g^2h^2)}{[1 - \exp(-2\pi^2g^2h^2)]^2 + 4\sin^2(\pi h)\exp(-2\pi^2g^2h^2)]}$$
$$= \frac{\sinh(q^2\sigma_L^2/2)}{\cosh(q^2\sigma_L^2/2) - \cos(Lq)} \quad (3)$$

where g is the so-called Hosemann's g factor and defined as $g = \sigma_L/L$. σ_L is a standard error of Gaussian distribution of L. h is defined as $h = Lq/2\pi$ [50]. As a result, the scattering intensity $I(q)$ is given by Eq. (4).

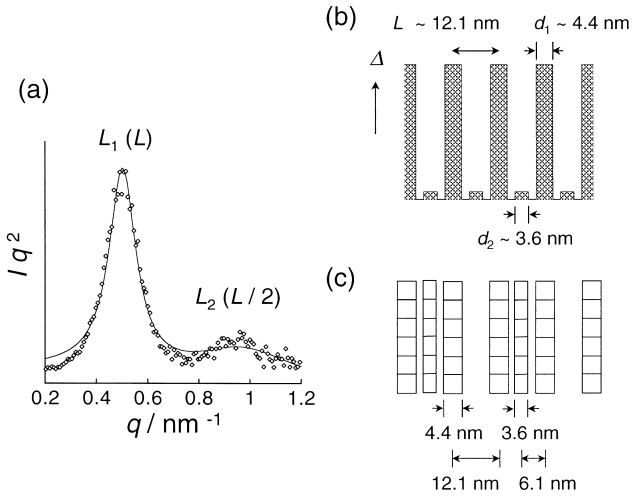

Fig. 11. (a) An example of curve fitting result for the SAXS profile taken in the isothermal crystallization process at 130 °C (at 1438 s). Open square: observed SAXS profile and solid line: calculated scattering intensity. (b) The corresponding lamellar structure model. More realistic model which gives essentially the same SAXS profile is given in (c).

$$I(q) = \frac{4[\Delta_1^2 \sin^2(d_1q/2) + 2\Delta_1\Delta_2 \cos(Lq/2)\sin(d_1q/2)\sin(d_2q/2) + \Delta_2^2 \sin^2(d_2q/2)]\sinh(q^2\sigma_L^2/2)}{q^2[\cosh(q^2\sigma_L^2/2) - \cos(Lq)]} \quad (4)$$

When the total number of these lamellar stacking structures is N_t, the actually observed scattering intensity $I_t(q)$ is given as

$$I_t(q) = N_tI(q) = N_t\frac{4[\Delta_1^2 \sin^2(d_1q/2) + 2\Delta_1\Delta_2 \cos(Lq/2)\sin(d_1q/2)\sin(d_2q/2) + \Delta_2^2 \sin^2(d_2q/2)]\sinh(q^2\sigma_L^2/2)}{q^2[\cosh(q^2\sigma_L^2/2) - \cos(Lq)]}$$
$$= \frac{4[(\Delta_1')^2\sin^2(d_1q/2) + 2\Delta_1'\Delta_2' \cos(Lq/2)\sin(d_1q/2)\sin(d_2q/2) + (\Delta_2')^2\sin^2(d_2q/2)]\sinh(q^2\sigma_L^2/2)}{q^2[\cosh(q^2\sigma_L^2/2) - \cos(Lq)]} \quad (5)$$

where $\Delta_1' = N_t^{1/2}\Delta_1$ and $\Delta_2' = N_t^{1/2}\Delta_2$.

The structural parameters in Eq. (5) were determined by carrying out the curve fitting of the observed SAXS profile. As an example, Fig. 11(a) shows the result of curve fitting for the data taken at 1438 s after the temperature jump to 130 °C. The calculated curve is in good agreement with the observed data indicated by open squares. In Fig. 11(b) is given the corresponding lamellar stacking model. Although it was impossible to obtain the electron density differences Δ_1 and Δ_2 directly as long as the N_t was not estimated definitely, we can discuss the relative magnitude of Δ_1 and Δ_2 from the evaluated Δ_1' and Δ_2' values in Eq. (5). The lamella generated in between the initially-created lamellae has the electron density difference Δ_2 of 1/16 the Δ_1, the electron density difference of the initial lamellae. This result can be interpreted in such another way that the structure of long period 6 nm is existent at an averaged probability of 1/16 or ca. 6% in the array of lamellae with 12 nm period, as illustrated in Fig. 11(c). In Fig. 9 the equivalency was pointed out between the regularly repeated lamellar model I and the randomly stacked lamellar model IV. As a trial and in order to show this equivalency concretely, the 100 types of randomly stacked lamellar models were generated in total by taking into account the probability of 1/16 to find the newly-inserted lamellae, where the total number of lamellae in one model was 40 (refer to Fig. 15 in a later section). The scattering profiles were calculated by Fourier-transformation of these models and were averaged to get a SAXS profile at 1438 s. The result is compared in Fig. 12 with the scattering profile derived for model I with the properly-adjusted parameters. Although the calculated profile (b) has

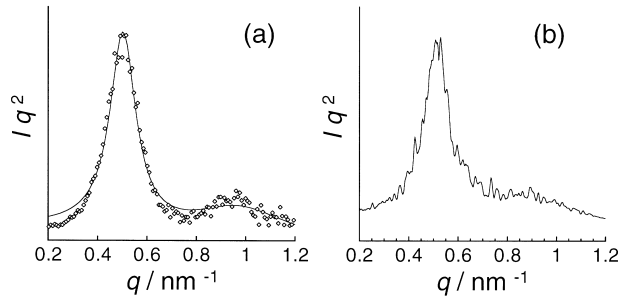

Fig. 12. Comparison between (a) the SAXS profile calculated for the model I in Fig. 9 with the parameters properly obtained from the observed data and (b) the SAXS profile averaged for the profiles calculated for 100 models of randomly stacked lamellar structure (model IV) with the inserted lamellar part at 1/16 probability. The open squares in (a) are the experimental data obtained at 130 °C at 1438 s.

small ripples due to the limited number of lamellae in the Fourier-transformation process, the agreement is nice between the two types of calculated profile.

In Fig. 13 is shown the thus-obtained time dependence of the electron density differences Δ_1' and Δ_2', the long period L, the thickness of lamellae generated in the first and second stages of crystallization, and the g factor. Immediately after jump, the lamellae with thickness of ca. 3 nm were generated at a long period of 14.5 nm. The lamellar thickness increased steeply in a short time and became almost constant. As seen from the rapid decrease in g factor, the stacking structure of lamellae was regularized in parallel to the thickening of lamellae and the decrease in long period. When the SAXS profiles given in Fig. 7 were investigated in detail, the profile changed gradually even in the time region before the appearance of peak L_2. For example, in the SAXS profile measured at 27 or 35 s a small and broad peak around $q = 1.1\ \mathrm{nm}^{-1}$ seems to be the third-order peak of the first L_1 peak. The second-order peak should be located on the shoulder of the L_1 peak because of the effect of paracrystalline disorder. With the passage of crystallization time the shoulder or the second-order peak became weaker and the third-order peak was clearer. According to the calculation given in Appendix A, the ratio of I_2/I_1 decreases and the ratio I_3/I_1 increases when the lamellar thickness d_1 increases in the range of $d_1 < L_1/2$, where I_i is the intensity of the ith order peak. In the time region of 50–100 s, the lamellar thickness d_1 was much smaller than the half of the long period and it increased with time as seen in Fig. 13. The observed behavior of the second- and third-order SAXS peaks (Fig. 7) is consistent with the above-mentioned prediction (Appendix A), although the comparison is only qualitative because of low signal-to-noise ratio.

In the second stage of crystallization, a new peak (L_2) started to appear and the third-order peak of the L_1 peak was difficult to observe any more. The thickness d_1 of the original lamellae was almost saturated and the thickness of the new lamellae was ca. 3.5 nm. The g value decreased furthermore but gradually with time. Fig. 14 shows the time

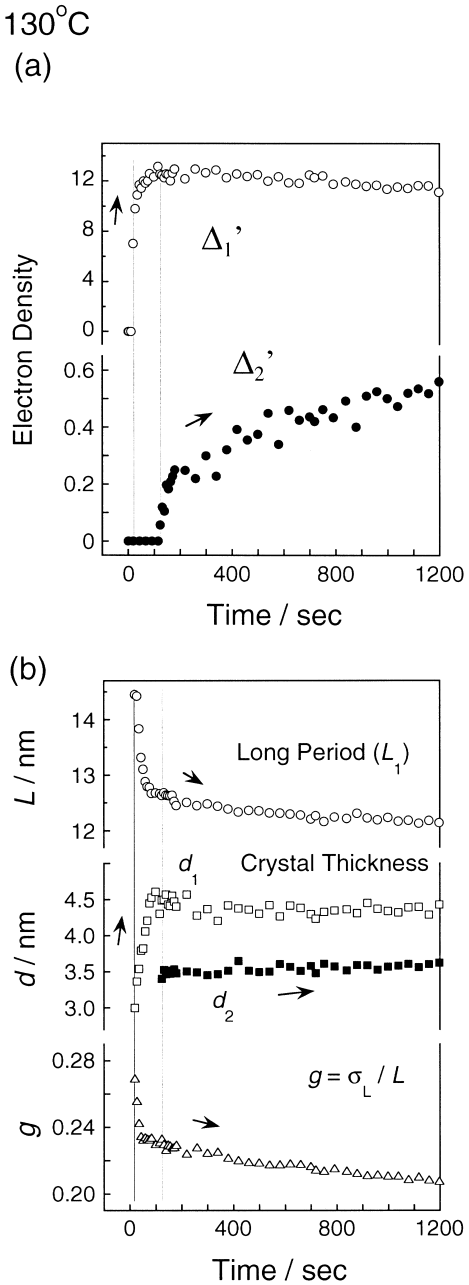

Fig. 13. Time dependence of the structure parameters of POM estimated in the isothermal crystallization process at 130 °C. (a) Time dependence of Δ_1' and Δ_2' and (b) time dependence of long period, crystal thickness and g factor.

evolution of stacked lamellar structure, where the information on lamellar thickness, etc. is given. With the passage of time, the electron density of the second new lamellae increased gradually. The Δ_2 height is not very high but only about 1/100–1/10 of the Δ_1 height at most. As pointed out in Fig. 9, these pictures may be redrawn by using statistically random lamellar stacking models given in Fig. 15.

In the case of isothermal crystallization at 150 °C, only the SAXS L_1 peak was observed and no L_2 peak was detected as shown in Fig. 8. The SAXS profile change seems consistent with the aforementioned prediction, that is, the

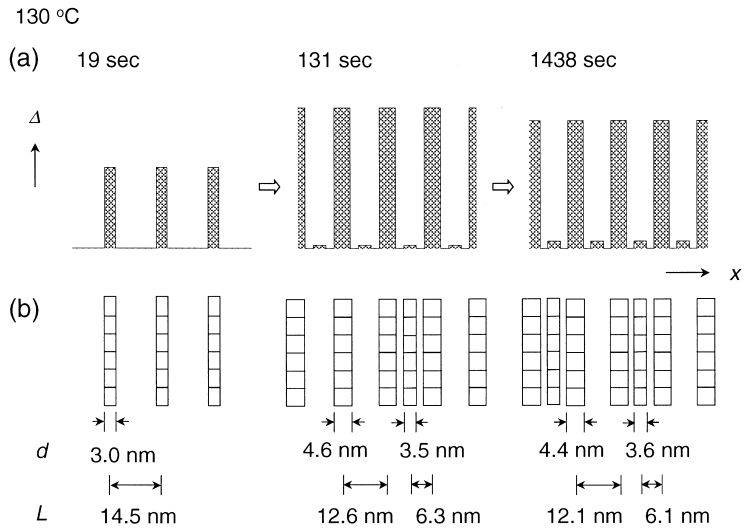

Fig. 14. Time dependence of lamellar stacking structure of POM in the isothermal crystallization process at 130 °C from the melt. (a) Time dependence of one-dimensional electron density profile and (b) an equivalent but more realistic lamellar stacking structure with stacked lamellar defect.

shoulder of the L_1 peak or the second-order peak became weaker and the L_1 peak became more symmetric, and the third-order peak increased the relative intensity although the peak was low, broad and noisy. Fig. 16 shows the time dependence of electron density Δ', long period L, crystal thickness d and g factor obtained by the curve fittings of the observed SAXS profiles, where the subscript '1' is erased for simplicity. The long period changed from 21 to 16 nm in a short time of 60 s after jump. The lamellar thickness was much larger than that at 130 °C, and increased steeply from 6.3 to 7.8 nm.

3.5. Combination of IR, SAXS and WAXS data

Fig. 17(a) and (b) show the temperature dependence of WAXS profile measured in the isothermal crystallization at 130 and 150 °C from the molten state, respectively. The integrated intensity of the crystalline (100) reflection was estimated as seen in Figs. 18 and 19. In these figures the long period estimated from the SAXS data and the intensities of the infrared bands characteristic of FCC and ECC are also plotted for comparison. These figures may be divided into several time regions. By comparing all these data, a structural evolution process may be deduced more concretely in the following way as illustrated in Figs. 20 and 21.

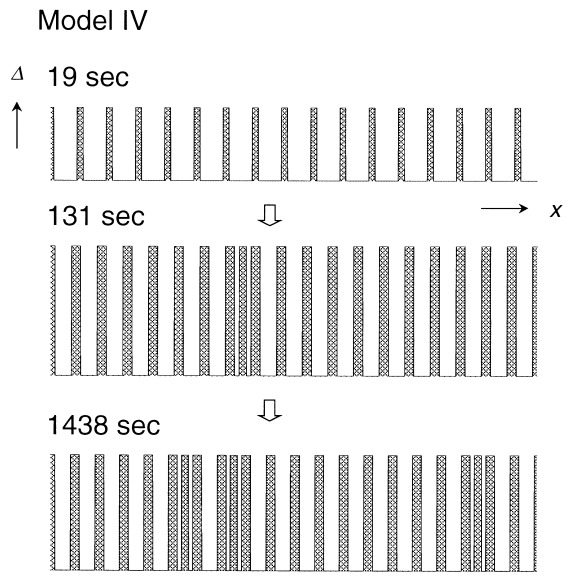

Fig. 15. Time evolution of lamellar stacking structure redrawn from Fig. 14.

3.5.1. Isothermal crystallization at 130 °C

Time Region I. Immediately after the sample was cooled steeply from the melt to 130 °C, the FCC lamellae of about 3.0 nm thickness started to appear and were stacked at an averaged long period of 14.5 nm. The intensity of the WAXS (100) reflection increased also steeply with time.

Time Region II. The long period of the stacked lamellae became shorter and reached almost the constant value, 12–13 nm. The lattice spacing estimated from the (100) reflection or the a-axial length of the unit cell was almost unchanged. Around 150 s the new lamellae of ca. 3.5 nm thickness started to appear at a long period of 6.3 nm. These new lamellae locate in between the already existing lamellae. At the same time the infrared bands intrinsic of ECC morphology were observed to increase in intensity. How can we combine the observation of ECC bands with the generation of new lamellae between the initially-stacked lamellae? As already discussed in the previous papers [29,30], we may speculate a generation of fully-extended chain stems, which pass through the several lamellae continuously, as illustrated in Fig. 20. These extended chain stems may correspond to the so-called taut tie chains. According to the theory about the frequency shift due to the dipole–dipole interactions, the vibrational frequency of the A_2 bands is a function of an R/H ratio of cylindrical crystallite [32]. The observed frequency position 902 cm^{-1} may

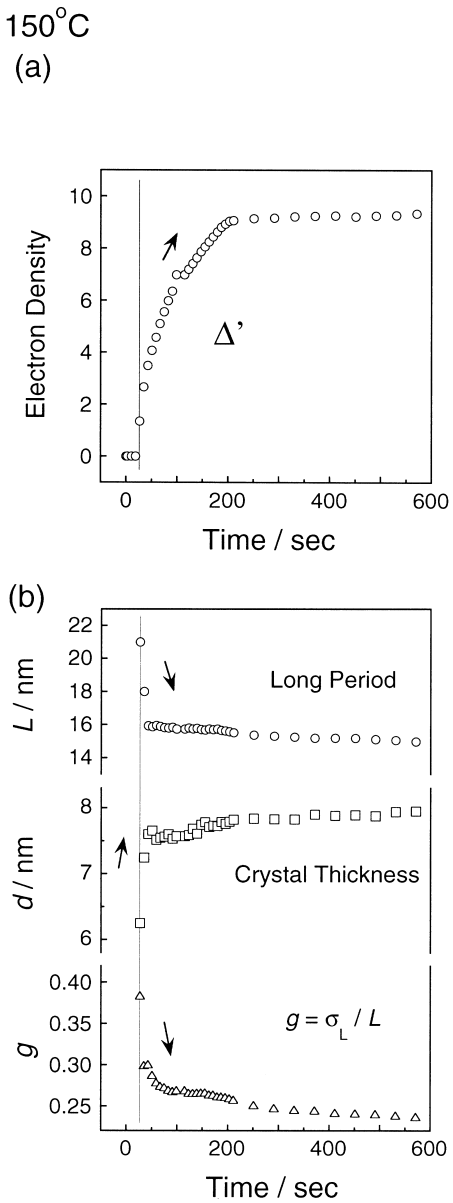

Fig. 16. Time dependence of the structure parameters of POM estimated in the isothermal crystallization process at 150 °C. (a) Time dependence of Δ' and (b) time dependence of long period, crystal thickness and g factor.

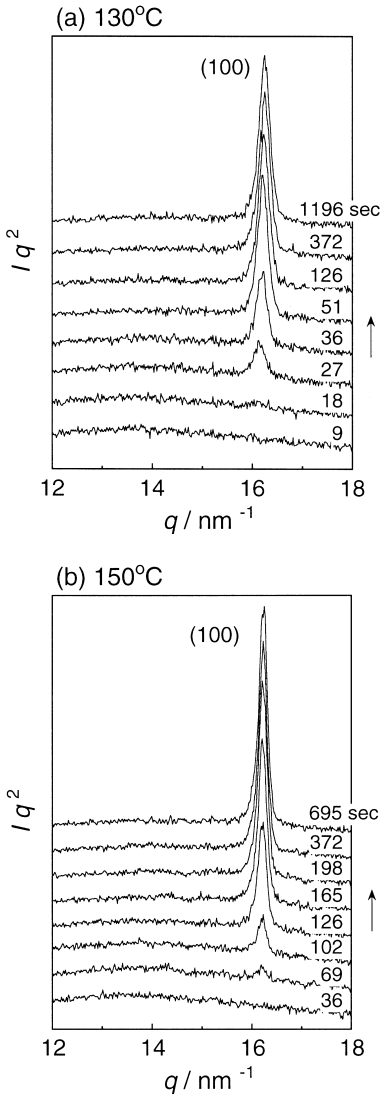

Fig. 17. Time dependence of the WAXS profile of POM sample measured in the isothermal crystallization process at (a) 130 °C and (b) 150 °C.

correspond to the R/H ratio of about 0.1. In Fig. 20 an extended chain stem passing through three lamellae has a length of ca. 20 nm. If this length is assumed as a cylinder height H, then the radius R is about 2 nm. That is to say, the taut tie chains of extended conformation is speculated to form a small bundle of cylindrical shape with 20 nm length and 2 nm radius.

Time Region III. When the crystallization time was beyond 650 s, the SAXS intensities of the L_1 and L_2 peaks and the intensities of the FCC and ECC infrared bands changed their slopes slightly as seen in Fig. 18. In particular, the infrared intensity of ECC band increased more remarkably, suggesting an increase of the number of taut tie chains. The integrated intensity of the (100) reflection changed also there but very slowly. All these findings suggest some additional change in the inner structure and/or the lamellar stacking mode, but the details are not clear at the present stage.

3.5.2. Isothermal crystallization at 150 °C

Structural evolution process is shown in Fig. 21.

Time Region I'. When the temperature jump was made from the melt to 150 °C, the chain-folded lamellae of about 6 nm thickness were found to appear at first, which were staked at an averaged long period of 21 nm. This structural formation occurred more slowly and in wider time region than the case of 130 °C. The infrared FCC band appeared in parallel to the SAXS L_1 peak and the WAXS (100) reflection.

Time Region I''. The long period of stacked lamellae was shortened and reached the almost constant value of 15–16 nm. The integrated intensities estimated for the WAXS

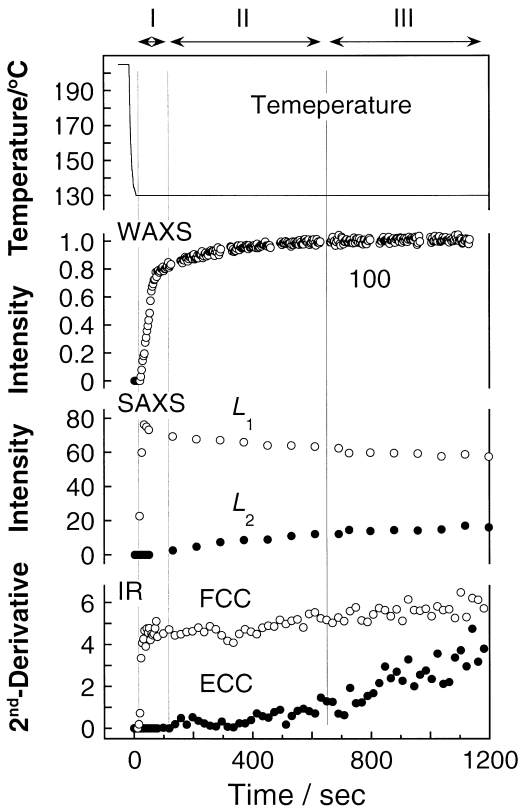

Fig. 18. Comparison of time dependence between the integrated intensity of WAXS (100) reflection, the intensity of the SAXS L_1 and L_2 peaks, and the infrared intensity of FCC and ECC bands (second derivatives) evaluated for the isothermal crystallization process at 130 °C.

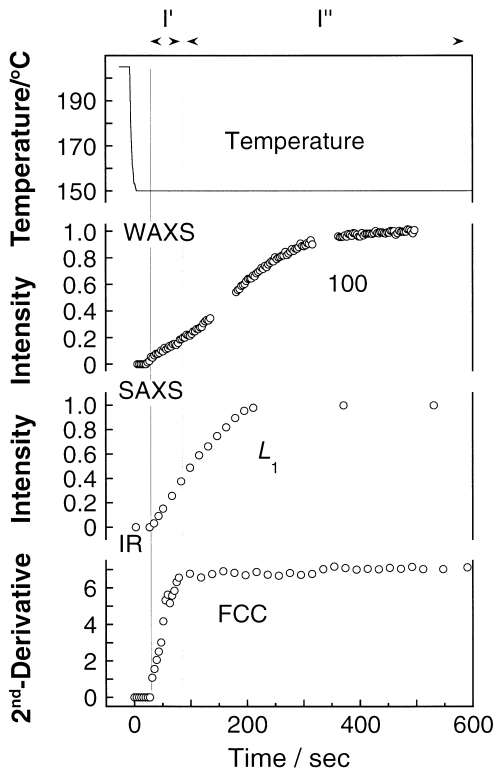

Fig. 19. Comparison of time dependence between the integrated intensity of WAXS (100) reflection, the intensity of the SAXS L_1 peak, and the infrared intensity of FCC band (second derivatives) evaluated for the isothermal crystallization process at 150 °C.

(100) reflection and the SAXS L_1 peak increased gradually. But the infrared FCC band intensity was almost saturated in this time region. The averaged lamella thickness was almost unchanged as shown in Fig. 16. Therefore it might be said that the helical chain segments in the crystal lattice were packed more densely and the lamellar stacking became more homogeneous and tighter without any generation of new lamellae.

3.5.3. Relation between isothermal and non-isothermal crystallizations

In the previous papers we reported the structural change occurring in the slow cooling process from the melt or in the non-isothermal crystallization process [29,30]. As shown in Fig. 12, the generation of stacked lamellae was observed around 155 °C and the lamellar insertion occurred below 140 °C. As detected in the infrared spectral measurement, the formation of taut tie chains occurred also below 140 °C. The structure extracted in that experiment may be assumed to be thermally-stabilized because the measurements were made step by step at constant temperatures on the way of extremely slow cooling process at ca. 0.3 °C/min [29,30]. When we compare the structural change as a function of time in the isothermal crystallization process at a constant temperature (T_c) with that estimated as a function of

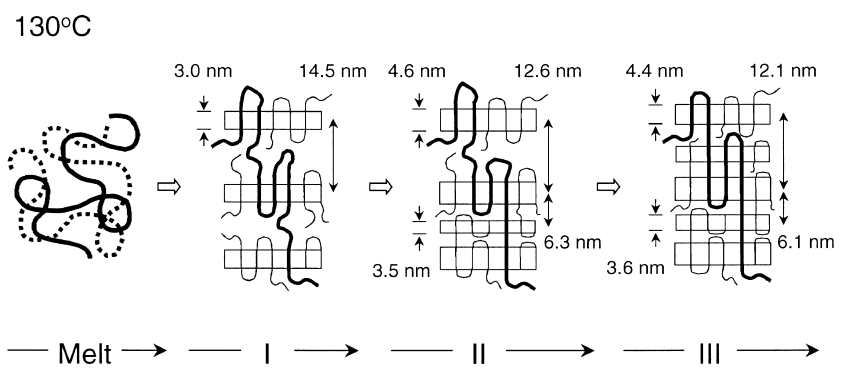

Fig. 20. Time dependence of the lamellar stacking structure and molecular chain conformation estimated in the isothermal crystallization process at 130 °C.

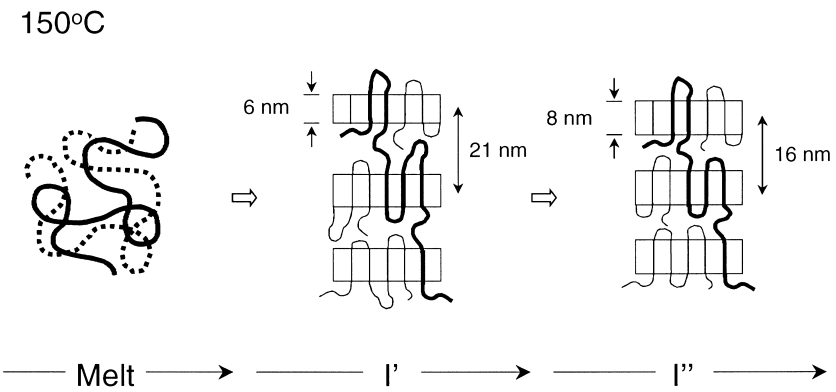

Fig. 21. Time dependence of the lamellar stacking structure and molecular chain conformation estimated in the isothermal crystallization process at 150 °C.

temperature in the slow cooling process, a series of structural change observed in the slow cooling process from the melt to T_c are realized successively on the way of the isothermal crystallization process. The structure attained after the passage of long time in the isothermal crystallization is equal to the structure detected at the corresponding temperature in the slow cooling process (Fig. 22): the structure detected at T_c in the slow cooling process is not created instantly even when the molten sample is brought suddenly to the T_c, but it is realized for the first time after passing many successive stages observed in the non-isothermal crystallization process in the temperature region higher than T_c. In other words, the structural evolution in the isothermal crystallization is considered to consist of many elementary processes such as the generation of isolated lamellae in the melt, the stacking of these lamellae, the insertion of new and thinner lamellae in between the original lamellae, the extension of tie chain segments to form the ECC-like structure, etc. The situation is quite similar to the chemical reaction consisting of many elementary processes. We might be able to develop a crystallization rate equation in terms of these elementary processes, just like the rate equation of chemical reaction.

A statement that the crystallization phenomenon consists of many elementary processes of microscopic structural level might be a commonsense. But, we wish to emphasize here that this important statement has been confirmed actually for the first time by carrying out the non-isothermal and isothermal crystallization experiments using the SAXS/WAXS and FTIR techniques and by comparing the concretely derived structural changes in both types of the crystallization processes.

4. Conclusions

In this paper, the structural evolution in the isothermal crystallization processes of POM was investigated at 130 and 150 °C from the melt by a combination of such various experimental techniques as DSC, FTIR, WAXS and SAXS. It should be emphasized here that the combination of these various techniques has allowed us to get quite concrete image of the structural evolution process in the crystallization. In particular, infrared spectra were quite useful for clarification of morphological change. By combining the IR data with the SAXS data, the existence of a bundle of taut tie chains was speculated, which pass through the several sheets of lamellae continuously. Another important point of the present paper is the interpretation of SAXS data. There were various plausible models to explain the observed SAXS profiles, but most of them were deleted and the lamellar insertion model was found to be the most reasonable. The SAXS data were quantitatively analyzed on the basis of scattering equations derived for the lamellar insertion model combined with the second-kind

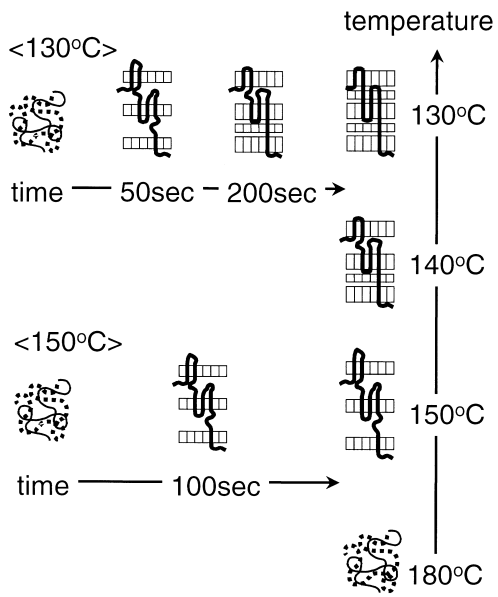

Fig. 22. Comparison between the structural change of POM extracted in the non-isothermal crystallization or slow cooling process from the melt and the structural evolution process estimated as a function of time in the isothermal crystallization process at 130 and 150 °C. The horizontal axis is time and the vertical axis is temperature. The structural evolution in the isothermal crystallization process at a temperature T_c is essentially the same as the structural change detected in the slow cooling process from the melt to T_c.

of paracrystalline disorder concerning the lamellar stacking regularity.

The structural change of POM is complicated: the lamellar stacking structure is changed in the primary (I) and secondary (II) crystallization processes. The stacked structure of crystalline lamellae at the initial stage of crystallization becomes tighter in the secondary stage by a generation of new lamellae in between the original lamellae. This lamellar insertion is not perfect but occurs at relatively low probability. That is to say, the lamellar stacks are consisted of two types of long periods, 6 and 12 nm. The stacking regularity is dependent on the crystallization temperature and more regular lamellar stacking structure is obtained at lower temperature [29,30]. This lamellar insertion mechanism is considered to be applicable to various kinds of polymers [34,40–49]. For example, polyethylene shows the lamellar stacking structure of ca. 80 nm long period in the early stage of crystallization, which is followed by the generation of new lamellae in between the original lamellae and the long period changes partly to 40 nm [34]. Judging from this similar lamellar insertion mechanism, we may expect that the taut tie chains might be existent also in the case of polyethylene. But, because of weak dipole–dipole interactions, the infrared spectra of PE are not sensitive to the shape of crystallite or morphology, different from the case of POM [32], and cannot tell us explicitly the existence of taut tie chains.

As easily speculated, the fully-extended chains may be produced by applying tensile or shear stress along the chain axis during the crystallization process. Typical example is a development of shish-kebab structure in the fiber spinning process [25,26]. By measuring the infrared spectra in this process, we might be able to trace the concrete growth of ECC and FCC regions in the fibers. The experiment is now going on through the combination of infrared method with the X-ray scattering technique.

Acknowledgements

The authors wish to thank Polyplastics Co. Ltd, Japan for kindly supplying POM sample.

Appendix A. SAXS profiles calculated for various lamellar stacking structures

As shown in the text (Fig. 7), the relative intensities of the SAXS peaks L_1 and L_2 changed as the crystallization was progressed. In order to choose the reasonable model for these observations, the effect of various parameters on the SAXS profile of stacked lamellar structure is investigated here.

A.1. Two-phases model

Crystalline lamellae and amorphous region are repeated as shown in Fig. A1(a). Using Eq. (1) in the text, the effects of total number of lamellae, lamellar thickness, lamellar stacking disorder and so on were investigated.

A.1.1. Total number of lamellae

As the total number of lamellae is increased, the scattering peaks become sharper and more intense, but the basic profile is not affected at all.

A.1.2. Lamellar thickness

As the lamellar thickness d is increased under the constant long period L, the relative intensity of the second-order peak (I_2) decreases gradually and becomes null at a point of $d/L = 1/2$, as shown in Figs. A1(b) and A2, where only the particle factor $P(q)$ was used in the calculation for simplicity. As the ratio becomes larger, the relative intensity

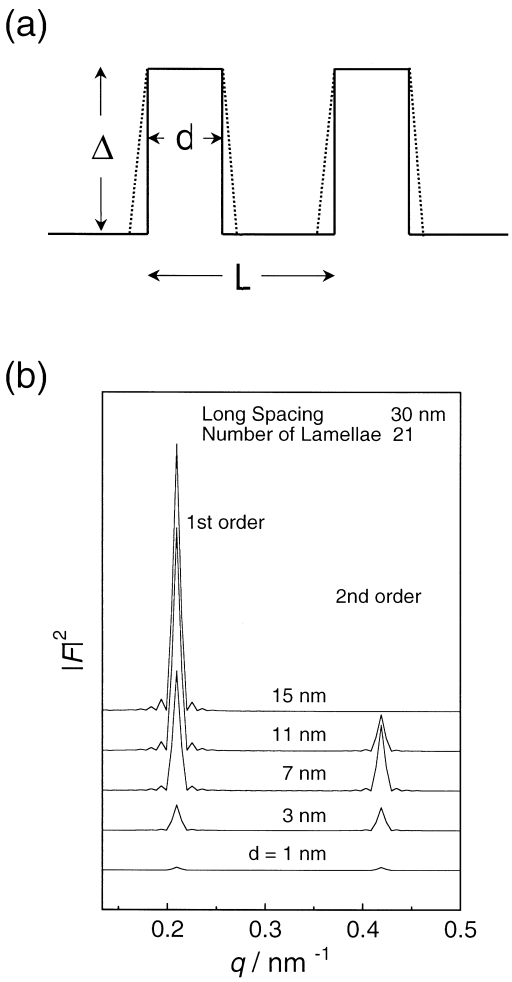

Fig. A1. (a) A two-phase model of stacked lamellae. The broken lines indicate the electron distribution in the interfacial boundary between the crystalline and amorphous regions. (b) The SAXS profiles calculated for the model with the various d values, where the long period L was fixed to 30 nm and the total number of lamellae was 21.

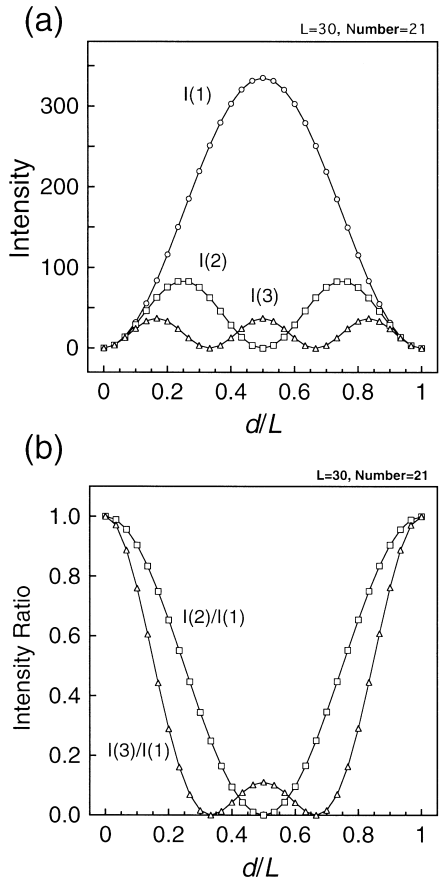

Fig. A2. (a) The scattering intensities of the first, second and third peaks of the SAXS profiles shown in Fig. A1(b). (b) The ratio of scattering intensities between the first, second and third peaks plotted against the ratio d/L.

increases again. The relative intensity of the third-order peak (I_3) changes also and shows the zero value at $d/L = 1/3$ and 2/3. These results are in agreement with those reported by Schultz et al. [39]. In the text, the discussion about the change in the second- and third-order peak intensities observed in Figs. 7 and 8 was made by focusing on the range of $d/L = 0.3–0.5$ in Fig. A2(b). The SAXS profile observed at 30 °C in the slow cooling process [30] was fitted using a particle factor $P(q)$ in Eq. (1) and the following parameters were obtained after the best fitting (Fig. A3): $L = 14.0$ nm, $d = 2.9$ nm, and $N = 2.0$. The total number of repeating lamellae $N = 2$ is quite unrealistic.

A.1.3. Stacking disorder

Paracrystalline disorder was introduced in the lamellar stacking mode. In this calculation the total number of lamellae was infinite, but the convolution of disorder between the adjacent lamellae resulted in the disappearance of stacking regularity in a finite range. The observed SAXS profile was fitted on the basis of Eq. (1) for the model shown in Fig. A1(a). The result is shown in Fig. A4, which is the same as that given in Ref. [30] (Fig. 9). The agreement between the calculated and observed profiles was not good.

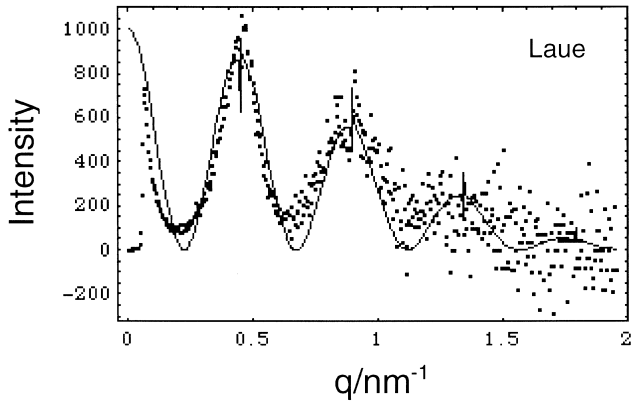

Fig. A3. Comparison between the observed (·) and calculated (- - -) SAXS profiles, where the particle factor $P(q)$ in Eq. (1) was used for the two-phase model shown in Fig. A1(a).

The parameters were $L = 14.0$ nm, $d = 2.6$ nm, and $\sigma = 3.1$ (The definition of σ is referred to in the text).

A.1.4. Effect of electron density distribution in the interfacial boundary

The electron density of the interfacial part between the crystalline and amorphous regions was assumed to change linearly as indicated by broken lines in Fig. A1(a). The calculated results were essentially the same as those mentioned above.

A.2. Lamellar insertion model

This model is shown in Fig. 10 in the text. At first only the particle factor $P(q)$ was taken into consideration in the curve fitting of the observed SAXS profiles, where the adjustable parameters were long period (L), total number of lamellae (N), and the relative electron density (Δ_i) and thickness (d_i) of the lamella i (= 1 and 2). The result was shown in Fig. A5, where $L = 13.0$ nm, $N = 2.0$, $\Delta_1 = 5.5$, $\Delta_2 = 2.9$, $d_1 = 5.4$ nm and $d_2 = 3.7$ nm. Similarly to the

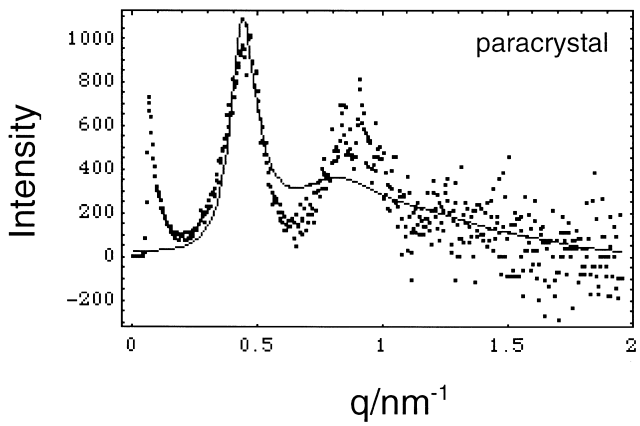

Fig. A4. Comparison between the observed (·) and calculated (- - -) SAXS profiles, where both the particle factor $P(q)$ and the lattice factor $L(q)$ in Eq. (1) were used for the two-phase model shown in Fig. A1(a) under the assumption of paracrystalline disorder of lamellar stacks.

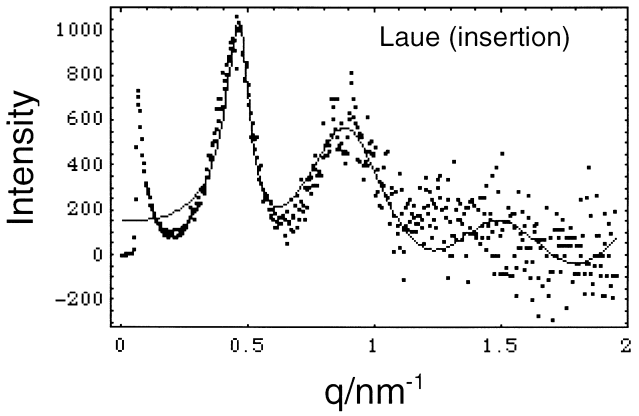

Fig. A5. Comparison between the observed (·) and calculated (- - -) SAXS profiles, where only the particle factor $P(q)$ in Eq. (1) was used for the lamellar insertion model shown in Fig. 10.

above-mentioned case (1), only the particle factor gave an unrealistically small number of repeating lamellae, $N = 2$. By an introduction of paracrystalline disorder ($L(q)$ in Eq. (1)) into the lamellar insertion model, for the first time, the comparatively good fitting of the observed SAXS profile and the physically reasonable parameters were obtained as described in the text (Fig. 11).

References

[1] Cutler DJ, Hendra PJ, Scerri ER, Cudby MEA, Willis HA. Polymer 1979;20:1470.
[2] Franbourg A, Rietsch F. Polym Bull 1990;24:445.
[3] Martin JA, Cruz-Pinto JJC. J Therm Anal 1993;40:621.
[4] Martin JA, Cruz-Pinto JJC, Oliveira MJ. J Therm Anal 1993;40:629.
[5] Cruz-Pinto JJC, Martins JA, Oliveira MJ. Colloid Polym Sci 1994; 272:1.
[6] Plummer CJG, Kausch H-H. Polym Bull (Berlin) 1994;32:117.
[7] Plummer CJG, Kausch H-H. Colloid Polym Sci 1995;273:227.
[8] Plummer CJG, Kausch H-H. Colloid Polym Sci 1995;273:719.
[9] Plummer CJG, Menu P, Cudre-Mauroux N, Kausch H-H. J Appl Polym Sci 1995;55:489.
[10] Phillips R, Manson J-AE. J Polym Sci, Part B: Polym Phys 1997;35: 875.
[11] Martins JA, Cruz Pinto JJC. Polymer 2002;43:3999.
[12] Geil PH. J Polym Sci 1960;47:65.
[13] Geil PH. J Polym Sci, Part C: Polym Lett 1966;13:149.
[14] Burmester A, Geil PH. In: Pae RD, Morrow DR, Chen Y, editors. Advances in polymer science and engineering. New York: Plenum Press; 1972. p. 42–100.
[15] Mihailov M, Terlemezyan L. Dokl Bolg Akad Nauk 1975;28:643.
[16] Salaris F, Turturro A, Bianchi U, Martuscelli E. Polymer 1978;19: 1163.
[17] Terlemezyan L, Mihailov M, Schmidt P, Schneider B. Makromol Chem 1978;179:807.
[18] Terlemezyan L, Mihailov M, Schmidt P, Schneider B. Makromol Chem 1978;179:2315.
[19] Terlemezyan L, Mihailov M. Makromol Chem 1978;179:2807.
[20] Schmidt P, Schneider B, Baldrian J, Terlemezyan L, Mihailov M, Ivanova B. Polymer 1987;28:217.
[21] Yeh F, Hsiao BS, Chu B, Sauer BB, Flexman EA. J Polym Sci, Part B: Polym Phys 1999;37:3115.
[22] Sauer BB, Hsiao BS, Wang Z-G. Polym Mater Sci Engng 1999;81: 361.
[23] Geil PH. Polymer 2000;41:8983.
[24] Sauer BB, Mclean RS, Londono JD, Hsiao BS. J Macromol Sci, Part B: Phys 2000;39:519.
[25] Samon JM, Schultz JM, Hsiao BS, Khot S, Johnson HR. Polymer 2001;42:1547.
[26] Samon JM, Schulz JM, Hsiao BS. Polymer 2002;43:1873.
[27] Hasegawa M, Yamamoto K, Shiwaku T, Hashimoto T. Macromolecules 1990;23:2629.
[28] Lucke A. Doctoral Thesis. Freiburg University; 1979.
[29] Hama H, Tashiro K. Polymer 2003;44:3107.
[30] Hama H, Tashiro K. Polymer 2003;44:2159.
[31] Shimomura M, Iguchi M, Kobayashi M. Polymer 1988;29:351.
[32] Kobayashi M, Sakashita M. J Chem Phys 1992;96:748.
[33] Tashiro K, Sasaki S, Kobayashi M. Polym J 1998;30:485.
[34] Sasaki S, Tashiro K, Kobayashi M, Izumi Y, Kobayashi K. Polymer 1999;40:7125.
[35] Tashiro K, Sasaki S. Prog Polym Sci 2003;28:451.
[36] Tashiro K, Izuchi M, Kaneuchi F, Jin C, Kobayashi M, Stein RS. Macromolecules 1994;27:1240.
[37] Tashiro K, Imanishi K, Izumi Y, Kobayashi M, Kobayashi K, Satoh M, Stein RS. Macromolecules 1995;28:8477.
[38] Kobayashi M, Sakashita M, Hasegawa M. Macromolecules 1991;24: 4796.
[39] Schultz JM, Lin JS, Hendricks RW. J Appl Cryst 1978;11:551.
[40] Geil PH. Bull Am Phys Soc 1962;7:206.
[41] Hoffman JD, Weeks JJ. J Chem Phys 1965;42:4301.
[42] Song HH, Stein RS, Wu DQ, Ree M, Phillips JC, LeGrand A, Chu B. J Polym Sci, Part B: Polym Phys 1988;21:1180.
[43] Song HH, Wu DQ, Chu B, Satkowski M, Ree M, Stein RS, Phillips JC. Macromolecules 1990;23:2380.
[44] Li Y, Jungnickel B-J. Polymer 1993;34:9.
[45] Hsiao BS, Gardner KH, Wu DQ, Chu B. Polymer 1993;34:3986.
[46] Hsiao BS, Gardner KH, Wu DQ, Chu B. Polymer 1993;34:3996.
[47] Lee CH, Saito H, Inoue T, Nojima S. Macromolecules 1996;29:7034.
[48] Dreezen G, Mischenko N, Koch MHJ, Reynaers H, Groeninckx G. Macromolecules 1999;32:4015.
[49] Akpalu YA, Amis EJ. J Chem Phys 2000;113:392.
[50] Hosemann R, Bagchi SN. Direct analysis of diffraction by matter. Amsterdam: North-Holland; 1962. p. 410.
[51] Hermans JJ. Recueil Trav Chim Pays-Bas 1944;63:5.
[52] Reinfold C, Fischer EW, Peterlin A. J Appl Phys 1964;35:71.
[53] Tsvankin DY. Polym Sci USSR 1964;6:2304.
[54] Blundell DJ. Acta Cryst Sect A 1970;26:472.
[55] Buchnan DR. J Polym Sci, Part A-2 1971;(9):645.
[56] Crist B. J Polym Sci Polym Phys Ed 1973;11:635.
[57] Bonart R, Muller EH. J Macromol Sci, Part B: Phys 1974;10:177.
[58] Beumer H, Hosemann R. J Macromol Sci, Part B: Phys 1978;15:1.
[59] Hosemann R, Hindelch AM. J Macromol Sci, Part B: Phys 1995;34: 327.